Giant Magnetoresistance in Hubbard Chains

Jian Li,[1] Chen Cheng,[1,*] Thereza Paiva,[2] Hai-Qing Lin,[1] and Rubem Mondaini[1,†]
[1]Beijing Computational Science Research Center, Beijing 100193, China
[2]Instituto de Física, Universidade Federal do Rio de Janeiro, Caixa Postal 68.528, 21941-972 Rio de Janeiro, Brazil

(Received 21 March 2018; published 11 July 2018)

We use numerically unbiased methods to show that the one-dimensional Hubbard model with periodically distributed on-site interactions already contains the minimal ingredients to display the phenomenon of magnetoresistance; i.e., by applying an external magnetic field, a dramatic enhancement on the charge transport is achieved. We reach this conclusion based on the computation of the Drude weight and of the single-particle density of states, applying twisted boundary condition averaging to reduce finite-size effects. The known picture that describes the giant magnetoresistance, by interpreting the scattering amplitudes of parallel or antiparallel polarized currents with local magnetizations, is obtained without having to resort to different entities; itinerant and localized charges are indistinguishable.

DOI: 10.1103/PhysRevLett.121.020403

Introduction.—The phenomenon of giant magnetoresistance highlights the speed in which some results in basic research can be rapidly converted into technological applications. It took less than a decade from its discovery in the late 1980s [1,2] to its implementation on the read heads of high-density hard disks commercialized for the general public. Specifically, it describes the significant reduction of electrical resistance of certain materials, composed of sandwiches of thin magnetic and nonmagnetic layers, in the presence of an external magnetic field. The physical explanation of this purely quantum mechanical effect relies on the fact that electrons traveling through a ferromagnetic conductor will scatter differently depending on the relative orientation of their spin to the magnetization direction of the conductor—with those oriented parallel scattering less often than those oriented antiparallel [3–5].

In a band picture, this is explained by the imbalance of charge populations with spin parallel and antiparallel to an external magnetic field, which translates into very different local density of states in the magnetic regions for both spin states at the Fermi energy [5]. For the antiparallel component, the reduced density of states results in a higher resistance for this channel, compared to a lower resistance for the parallel one. A simplified model of resistances, based on the scattering of each itinerant spin component by the magnetization of the background, qualitatively explains the increased conductivity in these materials since the external field polarizes the magnetization of the ferromagnetic layers, and it thus enhances the transport for electrons that have spin parallel to it [3–6].

Interestingly, this has also been investigated within the scope of *ab initio* electronic structure calculations, which do not account, *per se*, for interactions between electrons but are complemented by spin-dependent scattering using quasiclassical methods [7,8]. Here, our approach is different: We start from the simplest possible interacting model describing electrons hopping on a lattice with reduced dimensionality—essentially a one-dimensional chain or a nanowire—and model magnetic and nonmagnetic regions via site-dependent (although periodic) interactions. By unbiasedly calculating the transport properties of this simplified system, we show that it already contains the necessary attributes to display effects similar to the giant magnetoresistance (GMR) phenomenon in a purely interacting setting, as schematically represented in the sketch in Fig. 1. Besides, what is mostly considered a phenomenon that arises from the interplay of two types of electrons, localized and delocalized ones, here is obtained via a single entity.

Model and methods.—We use the one-dimensional Hubbard model with site-dependent interactions [9–14], creating a superlattice of size L,

$$\hat{\mathcal{H}} = -t\sum_{i,\sigma}(\hat{c}^{\dagger}_{i,\sigma}\hat{c}_{i+1,\sigma} + \mathrm{H.c.}) + \sum_{i} U_i \hat{n}_{i,\uparrow}\hat{n}_{i,\downarrow} - h\sum_{i}(\hat{n}_{i,\uparrow} - \hat{n}_{i,\downarrow}), \quad (1)$$

where $\hat{c}^{\dagger}_{i,\sigma}$ ($\hat{c}_{i,\sigma}$) creates (annihilates) a fermion with spin σ ($\uparrow$ or $\downarrow$) at the ith site of the lattice, and $\hat{n}_{i,\sigma} = \hat{c}^{\dagger}_{i,\sigma}\hat{c}_{i,\sigma}$. The first term in Eq. (1) accounts for the hopping of electrons between nearest-neighbor sites; U_i is the on-site Coulomb repulsion energy and h is the Zeeman energy related to an applied magnetic field $\vec{B}$. t sets the energy scale of the problem; we assume cyclic boundary conditions and restrict our results to half filling ($\sum_{i,\sigma}\langle\hat{n}_{i,\sigma}\rangle/L = 1$; $\langle\cdot\rangle$ is understood as the ground state average). For the interactions, we focus on the case where they are chosen in a periodic fashion with the repeated intercalation of the $U_i = U > 0$ and $U_i = 0$ sites [Fig. 1(a)].

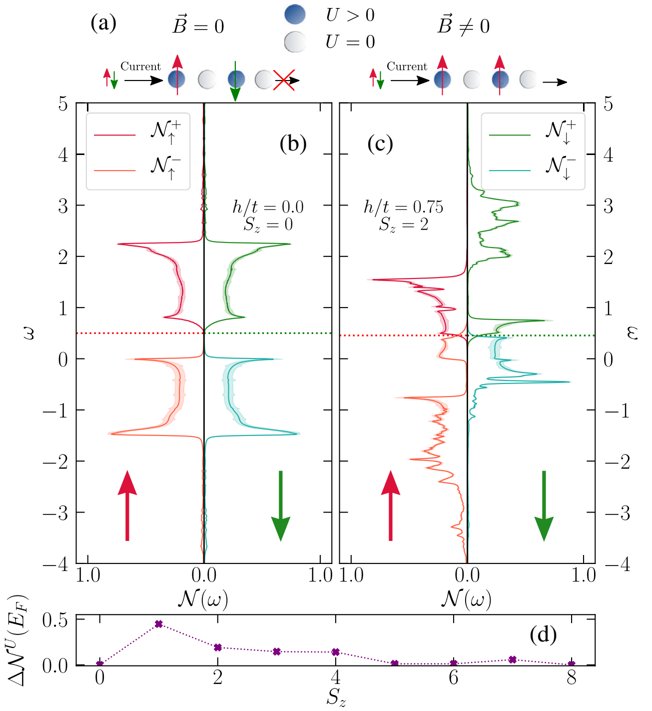

FIG. 1. (a) Schematic representation of the superlattice with the picture for transport and magnetism (see the text), in the absence or presence of an external magnetic field $\vec{B}$. In (b) [(c)], we display the spin-resolved density of states of the superlattice ($L = 16$) at zero temperature for $h = 0$ ($h \neq 0$). In the absence of the field, the Mott gap renders an insulating behavior, while the latter, a metal induced by the field, has a much higher mobility for charges with spin aligned to $\vec{B}$, as highlighted by the difference in local density of states at the Fermi energy for finite population imbalances in (d). Shading surrounding the curves depicts the error bars after the twisted boundary condition averaging and dashed lines, the Fermi energies.

To understand how this simple model leads to a crude interpretation of magnetic and nonmagnetic regions, it is useful to recall the dependence of the local moment, $\langle \hat{m}_i^2 \rangle \equiv \langle (\hat{n}_{i,\uparrow} - \hat{n}_{i,\downarrow})^2 \rangle$, on the interaction magnitude within a homogeneous lattice [inset of Fig. 2(a)]. Starting from the noninteracting regime, it assumes a value of 1/2, at this density, and steadily increases towards 1 when approaching the Heisenberg limit for large U. Thus, interactions induce the formation of magnetic moments, and when generalizing to a superlattice configuration, this is still the case, albeit less dramatically due to a natural density imbalance between repulsive and free sites [Figs. 2(a) and 2(b)]. This argument leads to the simple association that $U > 0$ and $U = 0$ types of sites can mimic the physics of magnetic and nonmagnetic regions in actual materials.

In what follows, we have used Lanczos diagonalization [15] and density matrix renormalization group (DMRG) [16,17] to obtain the ground state properties of the superlattices. We notice that when dealing with independent

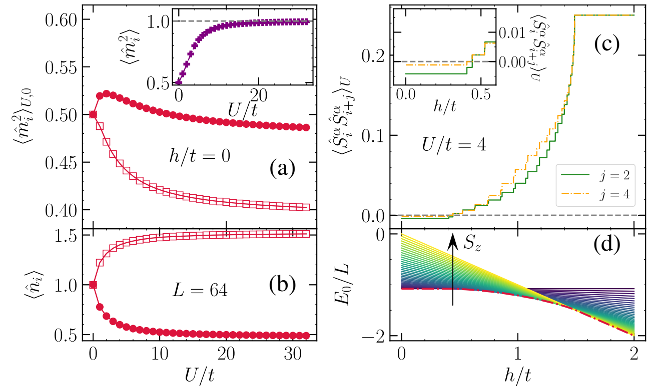

FIG. 2. Local moment $\langle \hat{m}_i^2 \rangle_U$ ($\langle \hat{m}_i^2 \rangle_0$) and its dependence on the interaction strength in repulsive (free) sites, marked by full (empty) symbols in (a), for the superlattice with $h/t = 0$. (Inset) The same for a homogeneous lattice; the dashed line denotes the Heisenberg limit of full localization. Site-dependent interactions break particle-hole symmetry and lead to an imbalance of the densities in both types of sites, as shown in (b). In (c), the spin correlations for nearest and next-nearest repulsive sites, taking a repulsive site as the reference, as a function of the external field magnitude with $U/t = 4$. (Inset) The negative correlations for $h = 0$. All results are presented for a lattice with $L = 64$, using DMRG. (d) Dependence on the Zeeman field of the lowest energy state for different S_z sectors of Eq. (1). The ground state is represented by the lower dashed-dotted curve enveloping the lines of each sector.

sectors of the Hamiltonian with a given total magnetization in the z direction, $S_z = \frac{1}{2}(N_\uparrow - N_\downarrow)$ (N_σ is the total number of particles with spin σ), the Zeeman energy is trivially accounted for and results in a shift of the energies for finite values of the external magnetic field. Thus, as h grows, different sectors will host the ground state of the Hamiltonian, as exemplified in Fig. 2(d).

Density of states.—To see how this space-dependent local moment affects the transport properties in Eq. (1) and connects our problem to the known phenomenology of the GMR effect, we obtain the density of states by computing single-particle excitations in the ground state. This is accomplished by numerically calculating dynamical quantities as the spectral function [18, 19], $A_k^\sigma(\omega) = \sum_n |\langle \psi_0 | \hat{c}_{k,\sigma}^\dagger | \psi_n^{N_\sigma - 1} \rangle|^2 \delta(\omega + (E_n^{N_\sigma - 1} - E_0)) + \sum_n |\langle \psi_0 | \hat{c}_{k,\sigma} | \psi_n^{N_\sigma + 1} \rangle|^2 \delta(\omega - (E_n^{N_\sigma + 1} - E_0))$, which describes the dynamical response of creating a fermion and a hole with momentum k and spin σ in the ground state $|\psi_0\rangle$ (with eigenenergy E_0) of the Hamiltonian; $|\psi_n^{N_\sigma \pm 1}\rangle$ ($E_n^{N_\sigma \pm 1}$) are eigenstates (eigenvalues) of the Hamiltonian with an added or removed electron. When summing up all possible momentum excitations, one recovers the actual density of states, $\mathcal{N}_\sigma(\omega) = (2/L)\sum_k A_k^\sigma(\omega) = \mathcal{N}_\sigma^+(\omega) + \mathcal{N}_\sigma^-(\omega)$, where we have resolved the contributions for electron and hole excitations in the last equality. To mitigate the influence of finite-size errors, we have employed twisted boundary condition averaging [20–22]; this has been used in a variety of contexts so as to approach the results in the thermodynamical limit with limited system sizes [25–29], and it has been shown [30] to be especially relevant for the case of dynamical quantities [22].

In Figs. 1(b) and 1(c), we report this quantity for $h = 0$ and $h \neq 0$, respectively, for $U/t = 4$, averaged among 64 boundary conditions. In the absence of an external field, the interactions, even if not present in every site, induce the formation of a Mott gap separating the lower and upper Hubbard bands; therefore, the ground state is a perfect insulator. Now, by applying an external magnetic field, the ground state no longer has the total $S_z = 0$, but, rather, finite values. For, say $h/t = 0.75$, single-particle excitations in the ground state, which has $S_z = 2$, display a *metallic* behavior [31]. Moreover, the difference in the local density of states of both spin channels in repulsive sites at the Fermi energy, $\Delta\mathcal{N}^U = \mathcal{N}^U_\uparrow - \mathcal{N}^U_\downarrow$ [22], shows that the transport is facilitated when there is a population imbalance [Fig. 1(d)]. Hence, if one injects a non-spin-polarized current in the superlattice [see Fig. 1(a)], the transport is enhanced, similar to the GMR effect, also realized in nanowires [32–34]. Now, this is one of the differences between the standard GMR and our results: In the actual experiments, the material, being metallic, possesses a finite conductivity which is enhanced by the application of a magnetic field. Here, we start from a perfect insulator and see that it induces metallic behavior. In other words, the model we investigate displays *perfect* magnetoresistance, provided the field is sufficiently large to induce a finite magnetization in the ground state.

Relative magnetization.—A further characterization of the similarity between our results and the GMR physics can be seen through spin correlations. We notice that, in the latter, transport is enhanced when the magnetization of consecutive ferromagnetic layers is made parallel. In Fig. 2(c), we show the dependence on the Zeeman energy of the spin-spin correlation $\langle \hat{S}^\alpha_i \hat{S}^\alpha_{i+j} \rangle_U \equiv (1/4)\langle m^\alpha_i m^\alpha_{i+j} \rangle_U$, where i is a repulsive site and j is either the nearest or next-nearest site, also with $U > 0$; α is the direction of the applied Zeeman field. We notice that, for the values of the field where we observe the enhancement on the transport via the analysis of $N(\omega)$, these spin correlations are positive, denoting parallel orientation, while they are slightly negative in its absence. The arrows in Fig. 1(a) schematically represent this situation.

Transport properties: Drude weight.—A robust way of checking the transport properties of quantum systems is via the Drude weight, $D/\pi e^2$, that measures the density of mobile charge carriers to their mass, or charge stiffness [35,36]; i.e., in the thermodynamic limit $D \neq 0$ $(D = 0)$ signals a metallic (insulating) behavior. This quantity appears in the real part of the $q = 0$ optical conductivity, $\sigma(\omega) = D\delta(\omega) + \sigma_{\mathrm{reg}}(\omega)$, as a weight for the singular behavior at zero frequency; it has also been shown by Kohn [37] that it can be computed from the change of the ground state energy E_0 to an applied flux Φ on the lattice as [38]

$$\frac{D}{\pi e^2} = L\left(\frac{\partial^2 E_0}{\partial \Phi^2}\right)\bigg|_{\Phi=0}, \tag{2}$$

being related to the induction of persistent currents in the system. The flux is introduced in the Hamiltonian (1) via a Peierls substitution on the hopping terms of the Hamiltonian, i.e., $-t\hat{c}^\dagger_{i,\sigma}\hat{c}_{i+1,\sigma} \to -te^{\mathrm{i}\phi}\hat{c}^\dagger_{i,\sigma}\hat{c}_{i+1\sigma}$ [23,35,36], where $\phi = \Phi/L$ [39]. It is important to highlight that these phases are of merely mathematical help and do not alter the external magnetic field introduced in the Zeeman term of Eq. (1), since the latter could be taken as perpendicular to the field associated to the flux Φ. Besides, they also do not change physical observables as, e.g., densities [38].

A typical dependence of the ground state energy of the superlattice with the flux Φ, for $S_z = 1$, is presented in the inset of Fig. 3(a), for different values of L. Lattices with $L = 4n$ (n is an integer) are known to display a paramagnetic response $(D < 0)$ [35]. For that reason, we focus on the absolute values of D and its dependence on the Zeeman field, in Fig. 3(a), for different system sizes to understand whether it can show signatures of the enhancement of transport as observed in the density of states. Likewise, Fig. 3(b) shows the corresponding difference in energy between the cases with periodic $(\Phi = 0)$ and antiperiodic boundary conditions $(\Phi = \pi)$, $\Delta E(0, \pi)$ by using DMRG calculations in much larger lattices. Since the difference in energies will be finite as long as the curvature of $E_0(\Phi)$ at $\Phi = 0$ is finite, provided there are no other local minima or maxima in $0 < \Phi < \pi$, it is suitable to track $\Delta E(0, \pi)$, as one deals only with real numbers in the

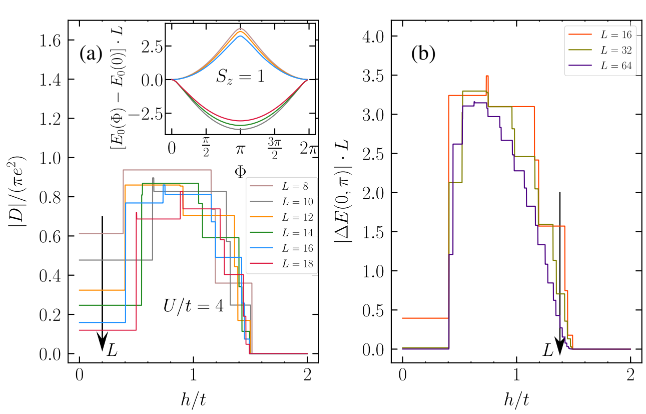

FIG. 3. (a) Drude weight dependence on the Zeeman energy for the superlattice with interaction strength $U/t = 4$ and different system sizes. These are obtained via Lanczos diagonalization after using Eq. (2) to obtain the curvatures of E_0L vs Φ curves; an example for zero field is presented in the inset. (b) The energy difference between periodic and antiperiodic boundary conditions for much larger system sizes obtained via DMRG as a function of the Zeeman energy.

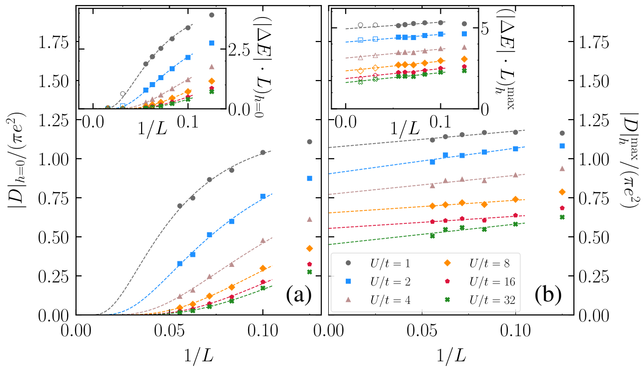

FIG. 4. System size scaling of the Drude weight in (a) the absence of a magnetic field and (b) for the value of h that results in the largest D for a given system size. (Insets) The respective scaling analyses for $\Delta E(0,\pi)$, where the empty symbols denote the DMRG results, for larger systems.

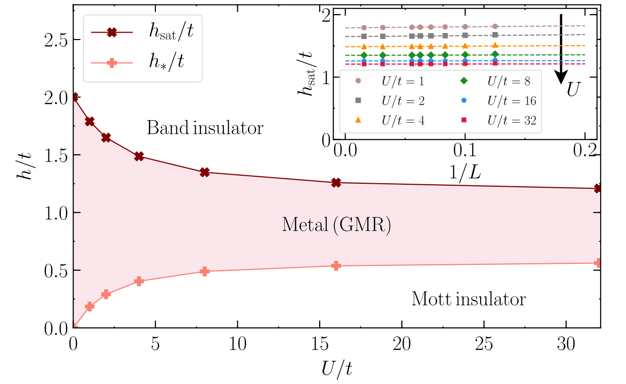

FIG. 5. Regime of parameters where the insulator-to-metal transition is observed (shaded area). Small (large) values of the field, result in a Mott (band) insulator. (Inset) The finite-size scaling of the saturation field, shown as an example. $h_{\rm sat}$ can be similarly obtained via an analysis of an effective two-body problem [22].

numerics. The qualitative behavior for the two quantities is similar: An initially finite and small Drude weight is suddenly increased after the ground state acquires a finite magnetization, for growing values of the field. At an even larger h/t, the transport decreases and the system becomes (band) insulating at a saturation Zeeman energy $h_{\rm sat}$. This corresponds to the situation where the ground state is fully polarized and the Pauli exclusion principle prevents any charge mobility.

A finite-size scaling is in order to assess the thermodynamic limit. We report in Fig. 4(a) the system size dependence of D at $h = 0$ and at the value of the field that gives the maximum Drude weight, $|D|_h^{\max}$; the insets display the same for $\Delta E(0,\pi)$ (with qualitative similar results), comparing a wide range of interactions U/t. In the former, we notice that, by using the functional form of Ref. [23], $|D| \propto \sqrt{L/\xi}e^{-L/\xi}$ (ξ is the Mott localization length), derived from the Bethe ansatz equations and thus valid for homogeneous chains, one can equally fit our data in the case of superlattices. Remarkably, half-filled superlattices possess insulating behavior when $L \to \infty$ in the absence of an external magnetic field, i.e., $D_{L\to\infty} \to 0$. On the other hand, for the maximum Drude weight, a linear extrapolation with $1/L$ results in finite D values [or $\Delta E(0,\pi)$]: The introduction of a magnetic field induces transport of the charges or, more precisely, an insulator-to-metal transition, for $h/t \approx 0.5$, and is particular to superlattices [22].

This is valid in the regime where U/t is finite since increasing the interactions leads to a smaller Drude weight in large lattices [Fig. 4(b)]. Apart from that, the enhancement of D in respect to the insulating case is constrained to regimes of finite magnetizations of the ground state other than $S_z = N_\uparrow/2 = L/2$. This generates a range of values of h/t where the magnetoresistance in our model can be manifest. Figure 5 analyzes how this range depends on the interaction magnitudes being limited by h_*, where the ground state no longer has $S_z = 0$, and $h_{\rm sat}$.

Summary and discussion.—We used a simple model, the Hubbard model with periodic site-dependent interactions under the presence of an external magnetic field, and we identify results analogous to the GMR phenomenon in a purely interacting setting. This is achieved via the identification of repulsive (noninteracting) regions as being magnetic (nonmagnetic), similar to the “sandwiches” of ferromagnetic and nonmagnetic layers in experimental samples. The combined quantification of transport and spin correlation functions show that when the magnetization in consecutive “magnetic” regions is made parallel due to the application of the magnetic field, the transport is enhanced, and an insulator-to-metal transition is obtained. An investigation of other densities and configurations of the superlattices may be relevant in the optimization of these features but goes beyond the scope of this Letter.

Most importantly, these results transcend the curiosity of solving a simple interacting model and have the possibility of being emulated using cold atoms trapped in optical lattices; charges and spin degrees of freedom are then translated into atoms and its hyperfine states, respectively. Besides, spatially dependent interactions are becoming a reality in experiments of ultracold gases. The usage of optical control to induce Feshbach resonances [40–44] and, consequently, local interactions, has witnessed new breakthroughs [45,46] that we envision being sufficient to investigate the space-dependent interactions of this model. Last, a verification of our results in experiments would require a precise quantification of transport of trapped atoms. Recently, however, this has been shown to be achievable when emulating the Hubbard model, either when focusing on spin [47] or charge [48] degrees of freedom. For this reason, our results may inspire experimentalists in understanding this highly unusual transport mechanism, which has a deep connection with the GMR effect, a phenomenon usually constrained to the condensed matter realm.

The authors acknowledge insightful discussions with R. R. dos Santos, P. D. Sacramento, G. Batrouni, R. T. Scalettar, and S.-W. Tsai. We acknowledge support by NSFC Grants No. U1530401 (J. L., C. C., R. M., and H.-Q. L.), No. 11674021 (C. C. and R. M.), and No. 11650110441 (R. M.); T. P. acknowledges the financial support of CNPq and INCT on Quantum Information. The computations were performed in the Tianhe-2JK at the Beijing Computational Science Research Center (CSRC).

[*]chengchen@csrc.ac.cn
[†]rmondaini@csrc.ac.cn

[1] M. N. Baibich, J. M. Broto, A. Fert, F. Nguyen Van Dau, F. Petroff, P. Etienne, G. Creuzet, A. Friederich, and J. Chazelas, Giant Magnetoresistance of (001)Fe/(001)Cr Magnetic Superlattices, Phys. Rev. Lett. **61**, 2472 (1988).

[2] G. Binasch, P. Grünberg, F. Saurenbach, and W. Zinn, Enhanced magnetoresistance in layered magnetic structures with antiferromagnetic interlayer exchange, Phys. Rev. B **39**, 4828 (1989).

[3] E. Gerstner, Nobel prize 2007: Fert and Grünberg, Nat. Phys. **3**, 754 (2007).

[4] P. A. Grünberg, Nobel lecture: From spin waves to giant magnetoresistance and beyond, Rev. Mod. Phys. **80**, 1531 (2008).

[5] Nobel Media AB, The Nobel prize in physics 2007—Advanced information, https://www.nobelprize.org/nobel_prizes/physics/laureates/2007/advanced.html.

[6] I. Žutić, J. Fabian, and S. Das Sarma, Spintronics: Fundamentals and applications, Rev. Mod. Phys. **76**, 323 (2004).

[7] P. Zahn, I. Mertig, M. Richter, and H. Eschrig, *Ab Initio* Calculations of the Giant Magnetoresistance, Phys. Rev. Lett. **75**, 2996 (1995).

[8] M. Richter, P. Zahn, M. Diviš, and I. Mertig, Giant magnetoresistance in uranium intermetallics: *Ab initio* calculations for U_2Pd_2In and U_2Pd_2Sn, Phys. Rev. B **54**, 11985 (1996).

[9] T. Paiva and R. R. dos Santos, Electronic Correlations in One-Dimensional Superlattices, Phys. Rev. Lett. **76**, 1126 (1996).

[10] T. Paiva and R. R. dos Santos, Metal-insulator transition in one-dimensional Hubbard superlattices, Phys. Rev. B **58**, 9607 (1998).

[11] T. Paiva and R. R. dos Santos, Magnetism in one-dimensional Hubbard superlattices, Phys. Rev. B **62**, 7007 (2000).

[12] T. Paiva and R. R. dos Santos, Charge-density waves in one-dimensional Hubbard superlattices, Phys. Rev. B **65**, 153101 (2002).

[13] A. L. Malvezzi, T. Paiva, and R. R. dos Santos, Multiperiodic magnetic structures in Hubbard superlattices, Phys. Rev. B **66**, 064430 (2002).

[14] L.-L. Zhang, J. Huang, C.-B. Duan, and W.-Z. Wang, Structure-dependent metal-insulator transition in one-dimensional Hubbard superlattice, Chin. Phys. B **24**, 077101 (2015).

[15] H. Q. Lin, J. E. Gubernatis, and Harvey Gould, Exact diagonalization methods for quantum systems, Comput. Phys. **7**, 400 (1993).

[16] S. R. White, Density Matrix Formulation for Quantum Renormalization Groups, Phys. Rev. Lett. **69**, 2863 (1992).

[17] S. R. White, Density-matrix algorithms for quantum renormalization groups, Phys. Rev. B **48**, 10345 (1993).

[18] E. R. Gagliano and C. A. Balseiro, Dynamical Properties of Quantum Many-Body Systems at Zero Temperature, Phys. Rev. Lett. **59**, 2999 (1987).

[19] E. Dagotto, Correlated electrons in high-temperature superconductors, Rev. Mod. Phys. **66**, 763 (1994).

[20] J. Tinka Gammel, D. K. Campbell, and E. Y. Loh, Jr., Extracting infinite system properties from finite size clusters: "Phase randomization/boundary condition averaging", Synth. Met. **57**, 4437 (1993).

[21] C. Gros, Control of the finite-size corrections in exact diagonalization studies, Phys. Rev. B **53**, 6865 (1996).

[22] See Supplemental Material at http://link.aps.org/supplemental/10.1103/PhysRevLett.121.020403, which includes Refs. [19,23,24], for an analysis on the twisted boundary averaging, finite size effects and a comparison with the homogeneous Hubbard model.

[23] C. A. Stafford, A. J. Millis, and B. S. Shastry, Finite-size effects on the optical conductivity of a half-filled Hubbard ring, Phys. Rev. B **43**, 13660 (1991).

[24] E. H. Lieb and F. Y. Wu, Absence of Mott Transition in an Exact Solution of the Short-Range, One-Band Model in One Dimension, Phys. Rev. Lett. **20**, 1445 (1968).

[25] S. Chiesa, P. B. Chakraborty, W. E. Pickett, and R. T. Scalettar, Disorder-Induced Stabilization of the Pseudogap in Strongly Correlated Systems, Phys. Rev. Lett. **101**, 086401 (2008).

[26] C. N. Varney, K. Sun, V. Galitski, and M. Rigol, Kaleidoscope of Exotic Quantum Phases in a Frustrated *XY* Model, Phys. Rev. Lett. **107**, 077201 (2011).

[27] T. Mendes-Santos, T. Paiva, and R. R. dos Santos, Size and shape of Mott regions for fermionic atoms in a two-dimensional optical lattice, Phys. Rev. A **91**, 023632 (2015).

[28] B. Schuetrumpf and W. Nazarewicz, Twist-averaged boundary conditions for nuclear pasta Hartree-Fock calculations, Phys. Rev. C **92**, 045806 (2015).

[29] M. Qin, H. Shi, and S. Zhang, Benchmark study of the two-dimensional Hubbard model with auxiliary-field quantum Monte Carlo method, Phys. Rev. B **94**, 085103 (2016).

[30] D. Poilblanc, Twisted boundary conditions in cluster calculations of the optical conductivity in two-dimensional lattice models, Phys. Rev. B **44**, 9562 (1991).

[31] The Fermi energies can be seen to be at the intersection of the single-particle excitation types, $\mathcal{N}_\sigma^+(\omega)$ and $\mathcal{N}_\sigma^-(\omega)$, and are verified through the calculation of the total number of particles for each spin species via integration of the spin-resolved density of states.

[32] L. Piraux, J. M. George, J. F. Despres, C. Leroy, E. Ferain, R. Legras, K. Ounadjela, and A. Fert, Giant magnetoresistance in magnetic multilayered nanowires, Appl. Phys. Lett. **65**, 2484 (1994).

[33] A. Blondel, J. P. Meier, B. Doudin, and J. Ph. Ansermet, Giant magnetoresistance of nanowires of multilayers, Appl. Phys. Lett. **65**, 3019 (1994).

[34] K. Liu, K. Nagodawithana, P. C. Searson, and C. L. Chien, Perpendicular giant magnetoresistance of multilayered Co/Cu nanowires, Phys. Rev. B **51**, 7381 (1995).

[35] R. M. Fye, M. J. Martins, D. J. Scalapino, J. Wagner, and W. Hanke, Drude weight, optical conductivity, and flux properties of one-dimensional Hubbard rings, Phys. Rev. B **44**, 6909 (1991).

[36] D. J. Scalapino, S. R. White, and S. Zhang, Insulator, metal, or superconductor: The criteria, Phys. Rev. B **47**, 7995 (1993).

[37] W. Kohn, Theory of the insulating state, Phys. Rev. **133**, A171 (1964).

[38] T. Giamarchi, *Quantum Physics in One Dimension*, International Series of Monographs on Physics Vol. 121 (Clarendon Press, Oxford, 2004).

[39] We use Peierls phases spread over each bond of the lattice so as to preserve translational symmetry, which is accounted for in the basis formation when using Lanczos ground state diagonalization. A trivial gauge transformation relates this case to the one with a single phase at the ends of the chain.

[40] D. M. Bauer, M. Lettner, C. Vo, G. Rempe, and S. Durr, Control of a magnetic Feshbach resonance with laser light, Nat. Phys. **5**, 339 (2009).

[41] R. Yamazaki, S. Taie, S. Sugawa, and Y. Takahashi, Submicron Spatial Modulation of an Interatomic Interaction in a Bose-Einstein Condensate, Phys. Rev. Lett. **105**, 050405 (2010).

[42] H. Wu and J. E. Thomas, Optical Control of Feshbach Resonances in Fermi Gases Using Molecular Dark States, Phys. Rev. Lett. **108**, 010401 (2012).

[43] H. Wu and J. E. Thomas, Optical control of the scattering length and effective range for magnetically tunable Feshbach resonances in ultracold gases, Phys. Rev. A **86**, 063625 (2012).

[44] A. Jagannathan, N. Arunkumar, J. A. Joseph, and J. E. Thomas, Optical Control of Magnetic Feshbach Resonances by Closed-Channel Electromagnetically Induced Transparency, Phys. Rev. Lett. **116**, 075301 (2016).

[45] L. W. Clark, L.-C. Ha, C.-Y. Xu, and C. Chin, Quantum Dynamics with Spatiotemporal Control of Interactions in a Stable Bose-Einstein Condensate, Phys. Rev. Lett. **115**, 155301 (2015).

[46] N. Arunkumar, A. Jagannathan, and J. E. Thomas, Designer spatial control of interactions in ultracold gases, arXiv:1803.01920.

[47] M. A. Nichols, L. W. Cheuk, M. Okan, T. R. Hartke, E. Mendez, T. Senthil, E. Khatami, H. Zhang, and M. W. Zwierlein, Spin transport in a Mott insulator of ultracold fermions, arXiv:1802.10018.

[48] P. T. Brown, D. Mitra, E. Guardado-Sanchez, R. Nourafkan, A. Reymbaut, S. Bergeron, A. M. S. Tremblay, J. Kokalj, D. A. Huse, P. Schauss, and W. S. Bakr, Bad metallic transport in a cold atom Fermi-Hubbard system, arXiv:1802.09456.